Tumor-Net: convolutional neural network modeling for classifying brain tumors from MRI images

Abu Kowshir Bitto [a,1,*], Md. Hasan Imam Bijoy [b,2], Sabina Yesmin [a,3], Imran Mahmud [a,4] , Md. Jueal Mia [b,5], Khalid Been Md. Badruzzaman Biplob [a,6]

[a] Department of Software Engineering, Daffodil International University, Daffodil Smart City, Dhaka, 1207, Bangladesh
[b] Department of Computer Science and Engineering, Daffodil International University, Daffodil Smart City, Dhaka, 1207, Bangladesh
[1] abu.kowshir777@gmail.com ; [2] hasan15-11743@diu.edu.bd; [3] sabina35-2406@diu.edu.bd; [4] imranmahmud@daffodilvarsity.edu.bd; [5] mjueal02@gmail.com; [6] khalid@daffodilvarsity.edu.bd
* corresponding author

ARTICLE INFO

Article history
Received July 18, 2022
Revised January 30, 2023
Accepted February 20, 2023
Available online April 7, 2023

Keywords
Brain tumor
MRI images
VGG16
VGG19
ResNet50

ABSTRACT

Abnormal brain tissue or cell growth is known as a brain tumor. One of the body's most intricate organs is the brain, where billions of cells work together. As a head tumor grows, the brain suffers damage due to its increasingly dense core. Magnetic resonance imaging, or MRI, is a type of medical imaging that enables radiologists to view the inside of body structures without the need for surgery. The image-based medical diagnosis expert system is crucial for a brain tumor patient. In this study, we combined two Magnetic Resonance Imaging (MRI)-based image datasets from Figshare and Kaggle to identify brain tumor MRI using a variety of convolutional neural network designs. To achieve competitive performance, we employ several data preprocessing techniques, such as resizing and enhancing contrast. The image augmentation techniques (E.g., rotated, width shifted, height shifted, shear shifted, and horizontally flipped) are used to increase data size, and five pre-trained models employed, including VGG-16, VGG-19, ResNet-50, Xception, and Inception-V3. The model with the highest accuracy, ResNet-50, performs at 96.76 percent. The model with the highest precision overall is Inception V3, with a precision score of 98.83 percent. ResNet-50 performs at 96.96% for F1-Score. The prominent accuracy of the implemented model, i.e., ResNet-50, compared with several earlier studies to validate the consequence of this introspection. The outcome of this study can be used in the medical diagnosis of brain tumors with an MRI-based expert system.

1. Introduction

The unnatural growth of brain tissue or cells is referred to as a brain tumor [1]- [4]. When malignancy grows in the head, the weighted interior of the brain expands, causing damage to the brain. An intracranial neoplasm, often a brain tumor, is a disorder where unexpected cells grow in the human brain. Two varieties of brain tumors exist malignant (cancerous) and benign (noncancerous). Tumors that cause cancer might be primary, metastases, or secondary tumors. When the DNA of normal brain cells has a flaw, it results in brain tumors. As we know, cells in the body constantly split and die, only to be replaced by another cell. Modern cells are formed in several circumstances, but the old cells are eliminated. These cells coagulate as a result, and they have the potential to form tumors. Brain tumors are frequently passed down through the generations. Gliomas are the most prevalent and powerful [5], [6]. Glioma detection at an early stage is critical for achieving the best treatment results [7]. Computed Tomography (CT), Attractive Resonance Imaging (MRI), etc. provide essential details on brain tumors'

form, size, location, and digestive system. While these modalities are used in combination to provide the most detailed information about brain tumors, MRI is considered the standard strategy due to its significant delicate tissue differentiation and broad accessibility [8], [9].

Many papers, publications, and research projects focus on detecting and categorizing brain tumors from MRI images. The study of Pereira *et al.* [2] described a CNN-based approach for segmenting brain tumors in MRI images. In order to accommodate deeper architectures, the CNN is constructed using small 3 3 kernels over convolutional layers. Brain Tumor Division identified a few strategies for producing a parametric / non-parametric classification of the fundamental architecture data in this article. These models frequently include probability work compared to perceptions and a prior model. Preprocessing, classification by CNN, and post-processing are the three key parts of the approach. The BRATS 2013 and 2015 databases were used to test the suggested technique. Be-cause brain tumors vary greatly in their spatial placement and basic composition; researchers have looked into the use of data increase to deal with this inconstancy. They looked at expanding our prepared data collection by pivoting patches and inspecting underrepresented HGG classes in LGG. The authors of a research by Deepak *et al.* [10] classified the three most common forms of brain tumors—gliomas, meningiomas, and pituitary tumors—into three different categories. Deep transfer learning and a Google Neural Network that had been trained to extract characteristics from brain MRI data were used in their suggested classification strategy. The authors extracted features using a pre-trained VGG-16 and fine-tuned AlexNet models. Support vector machines were then used to classify the features (SVM). Knowledge transfer was the foundation of the 3D CNN architecture used in the learning process. The accuracy metrics specified in their study were used by the authors to compare their transfer learning-based strategy with hand-crafted feature engineering.

Talo *et al.* [11] proposed a procedure for mechanically categorizing functional and dysfunctional brain MR pictures using deep learning. MR imaging is a well-known non-invasive technique for measuring neuronal movement in the brain of a human. MR pictures offer a huge unrealized for providing important data about numerous brain disorders' mentality, analysis, genetic characteristics, hemodynamics, and chemistry. ResNet34, Convolutional neural networks (CNNs) are the foundation of a deep learning model, is also used. The PSO SVM classifier with a basis function radial kernel was used with the Res-Net34 model, and it successfully identified brain anomalies. The experiments in this paper were carried out using the Harvard Medical School MR dataset, and numerous sophisticated deep learning approaches for hyperparameter optimization were used. Ahuja *et al.* [12] proposed employing the super pixel approach to detect and segment brain tumors via transfer learning. For starters, MRI cuts are divided into three categories: particular, typical, LGG, and HGG. Utilizing VGG-19 at epoch-6, the proposed methodology consistently produced validation data precision of 99.82 percent and 96.32 percent. The LGG and HGG MRI brain tumor pictures now used for segmenting the tumor. The super-pixel approach is used to divide tumors. The tumor segmentation yields a 0.932 normal dice file. The technique should be tested on a real-time patient database in the future. Supporting advancement in preprocessing procedures in division organizations is essential to raise the average dice list's quality. Khan *et al.* [13] describe a totally automatic profound learning method for multifunctional brain tumor classification that includes differentiating enhancement. The work's quality was graded in three stages. To begin, differentiation extending using the edge-based interface; he was used to prolong the image contrast of the tumor region in the preprocessing step. Furthermore, the use of general underlined the option of robust deep learning. Finally, the ELM classification was updated to categorize reported tumors into the appropriate group. This research extracted features derived from two various CNN models using transfer learning, and the synthesis was done. The goal of combining two CNN models was always to create a more modern include variable with more data. The test was run on the BraTs datasets, and the results showed an increase in precision (98.16 percent, 97.26 percent, and 93.40 percent, respectively, for the BraTs2015, BraTs2017, and BraTs 2018 datasets).

Kaur *et al.* [14] evaluated various pre-trained deep convolutional neural network (DCNN) models with TLCs for MR brain image prediction. The authors achieved high recognition accuracy by employing pre-trained DCNN models and exchange learning. Among the models tested, AlexNet

performed the best, with 100%, 94%, and 95.92% classification rates for all datasets. Their findings suggest that the use of pre-trained DCNN models and exchange learning can significantly improve the accuracy of MR brain image classification. They arose due to existing conventional and deep learning algorithms based on the categorization of brain tasks. In contrast, the author describes next work that will concentrate on running models on frameworks with GPU-enabled capacity, which is anticipated to reduce computational overhead and investigate various fine-tuning techniques. Khan *et al.* [13] describe an automatic multimodal classification technique for bra based on deep learning for brain tumor type categorization. Cancerous and noncancerous brain tumors exist [15]. It has the potential to injure the brain, which might be fatal. This study used a direct distinguish upgrade technique modified with the help of histogram equalization. The extracted features from two different CNN models were done via exchange learning, and the integration was done. The goal of combining two CNN architectures was to provide more data to an underused highlight vector.

According to the current state-of-art of categorization scheme for identifying brain tumors, there are more than 120 different types of brain tumors that vary in their origin, range, size, and features. This raises the chance of tumors, which can be caused by a genetic disorder called neurofibromatosis, furthermore exposure to chemicals like vinyl chloride, Epstein-Barr virus, and ionized radiation. Our study article's main objective is to determine how to employ transfer learning based on deep learning to identify the tumor from MRI pictures. The method of leveraging the information gained through a planned demonstration to acquire a new set of facts is known as transfer learning [16]. The transfer learning method is called inductive trade learning when labeled data is present inside the source and target areas for a classification problem [17]. Brain magnetic reverberation imaging (MRI) is one of the most trustworthy imaging modalities that analysts rely on for diagnosing brain malignancies and predicting tumor growth, both in the detection and therapy stages [18]. To contribute on previous studies, this study developed numerous computational techniques for brain tumor detection and classification utilizing brain MRI images since it became possible to channel and stack meaningful images to the computer. For the category and location of tumors, a CNN-based multi-task classification is built. We used Kaggle and Figshare datasets for this study. A total of 7138 brain MRI scans have been divided into four categories: pituitary, meningioma, glioma, and no tumor, where the CNN pre-trained model will be used.

The remainder of the paper is provided below. The proposed methodology for detecting brain tumors is described in Section 2, the results are shown and discussed in Section 3, along with a comparison of the methods used in Section 3, and the study is concluded in Section 4.

2. Method

The main goal of our study is to develop a deep learning-based transfer learning classifiers (TLCs) model that can distinguish tumors from MRI images. We must go through numerous phases to attain our aim, including dataset collecting, data preprocessing, model creation, etc. In Fig. 1, the functioning procedure is presented.

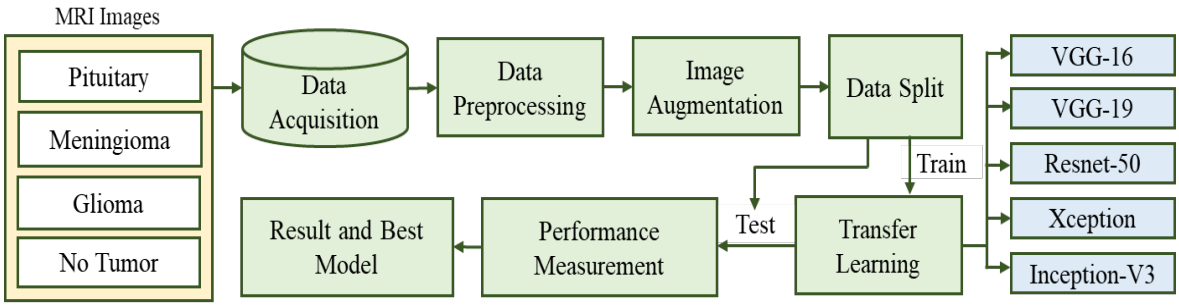

Fig. 1. Working procedure diagram to classify the brain tumor disease from MRI images

2.1. Dataset Description

We used Figshare and Kaggle to obtain brain tumor data from MRI images [19]. This dataset has 7138 brains MRI pictures, divided into four categories: pituitary, meningioma, glioma, and no tumor. Unusual growths that form in the pituitary gland are known as pituitary tumors. The size of a pea, this gland is an organ. It is situated near the base of the brain, behind the nose. Some of these tumors cause the pituitary gland to produce excessive hormones regulating vital bodily processes. One kind of tumor that develops close to the brain is a meningioma. While most of these tumors are benign (around 90%), some develop into a malignancy. Cell growth, known as a glioma, begins in the brain or spinal cord. Glial cells, which are healthy brain cells, resemble the cells in gliomas. Glial cells support nerve cells' functionality by surrounding them. A tumor is a mass of cells that develops when a glioma expands. Colors have been applied to the photographs taken, and example data has been presented in Fig. 2.

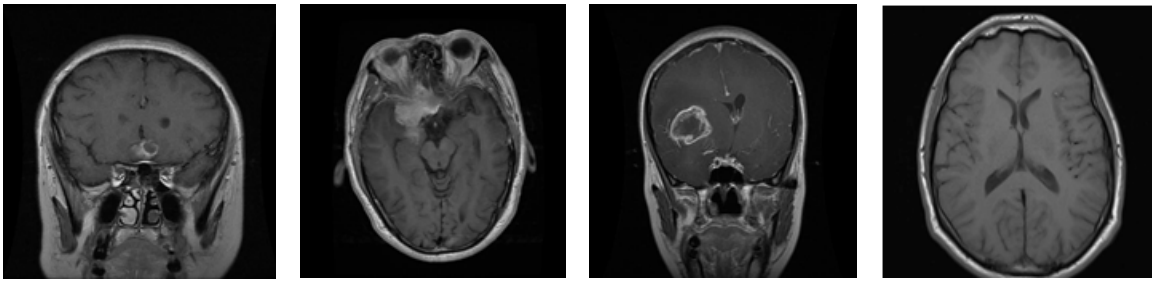

(a) Pituitary (b) Meningioma (c) Glioma (d) No Tumor

Fig. 2. Sample dataset for (a) Pituitary, (b) Meningioma, (c) Glioma and (d) No Tumor

2.2. Data Processing

Methods for data preparation use geometrical modifications. Scale, or image normalization, is used to map the data between an input image and an output image with a set of aligned image pairs for model development. The translation is used to map the data between an input image and an output image. Rotation is also used to correct the direction for the used accurate dimension of the image. The data resolution was lowered during the whole planning process. The picture pixels are 220x220 for VGG-16, VGG-19, ResNet-50, Xception, and Inception-V3. The quality of each photograph is the same high standard. The images were rotated, sheared, moved in width and height, and horizontally flipped based on the changes to the images.

2.3. Model Implementation

This study used the Convolutional Neural Network (CNN) based transfer algorithm for the brain tumor dataset. Transfer learning models relevant theory given below.

Transfer supervised machine-learning approach in which a show made for an errand is used as the project focusing on a significant task [20], [21]. Given the enormous computation, it is a common method in DL to use pre-trained algorithms as the preliminary step on computer vision and normal language-generating assignments. In computer vision, neural systems ordinarily point to identify edges within the first layer, shapes within the center layer, and task-specific highlights within the last-mentioned layers. The early and central layers are utilized in transfer learning, and the areas of the last-mentioned layer were retrained. It makes use of the named information from the errand it was prepared on.

VGG-16 (Fig. 3) is highly appealing because of its architecture, consisting of 16 convolutional layers [22]. There are many filters but only 3×3 convolutions, which makes it very close to AlexNet. On four GPUs, it might be taught for two to three weeks. However, it is currently the most widely used technique in the neighborhood for extracting information from pictures. Open-source feature extractors have used the VGG weight setting as a starting point in a range of other applications and problems. However, managing VGG might be challenging due to its 138 million parameters [23]. Gaining VGG is possible

through transfer learning. The model has already been trained on a dataset, the parameters have been tweaked for greater accuracy, and the parameter values can be applied.

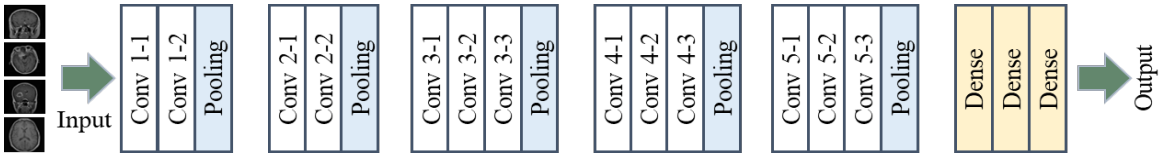

Fig. 3. VGG-16 block/architecture diagram

The VGG-19 architecture [24] consists of five convolutional blocks, which are implemented by three fully linked layers (Fig. 4). Following each convolution, an enhanced direct unit (ReLU) is developed, and the spatial dimension is then minimized at intervals using the max-pooling technique. To guarantee each physical measurement of the layer of neurons from the preceding layer is isolated, max-pooling layers use 2×2 sections with a walk of 2 and no cushioning. Currently employing the ultimate 1,000 fully softmax layer are two wholly connected layers with 4,096 ReLU enacted units. Extraction layers, which can be thought of as a subset of them, are included in convolutional components. The bottleneck characteristics are produced by the actuation maps produced by these layers.

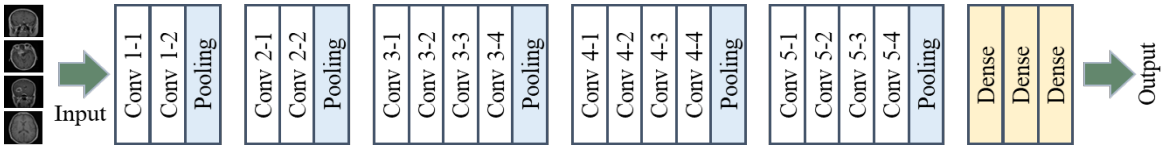

Fig. 4. VGG-19 block/architecture diagram

ResNet-50 (Fig. 5) is a CNN architecture, which is a variant of the ResNet model and is also known as a "Residual Neural Network" [25], [26]. ResNet50 is capable of processing up to 50 neural network layers. The ResNet50 architecture includes one MaxPool layer, one Normal Pool layer, and 48 Convolution layers. The model is known for its high computational performance, with 3.8×10^9 floating-point operations.

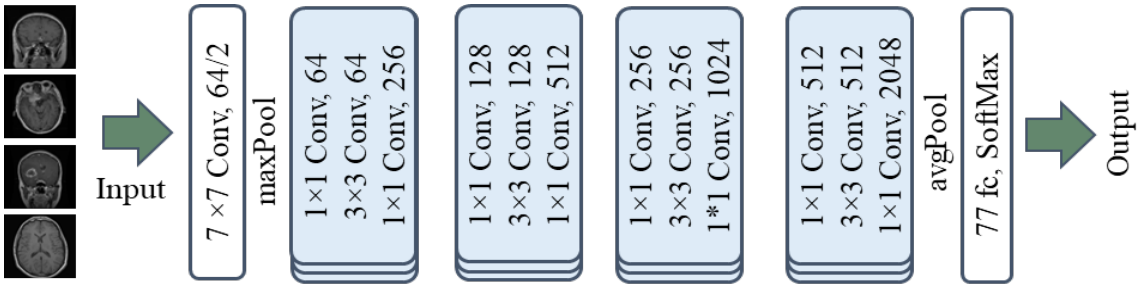

Fig. 5. ResNet-50 block/architecture diagram

Xception uses a 71-layer CNN-based architecture (Fig. 6). By loading a pre-trained network that has been trained on more than a million photos from the ImageNet database, the Xception model uses transfer learning. The Inception architecture has been changed to become Xception [27], where depth-wise Separable Convolutions have taken the role of the fundamental Inception modules. This change provides for better performance and more efficient calculation.

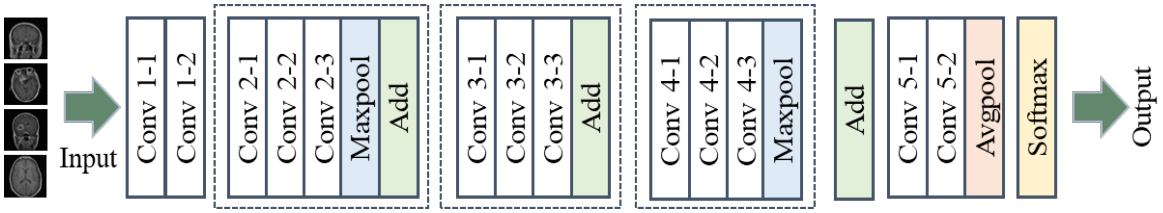

Fig. 6. Xception block/architecture diagram

The Inception Net (Fig. 7) is a CNN-based architecture that introduced a new standard for CNN classifiers by improving performance and accuracy while maintaining computational efficiency [28]. Inception Modules were developed to address over-fitting and computational expense by reducing dimensionality with stacked 1×1 convolutions, which enabled more efficient computation and deeper networks. The Inception Module consists of multiple layers, including 1×1 Convolutional Layer, 3×3 Convolutional Layer, and 5×5 Convolutional Layer. The output filter banks of each layer are combined into a single output sequence, which serves as input for the next phase. This approach helps to improve accuracy and computational efficiency in CNN classifiers.

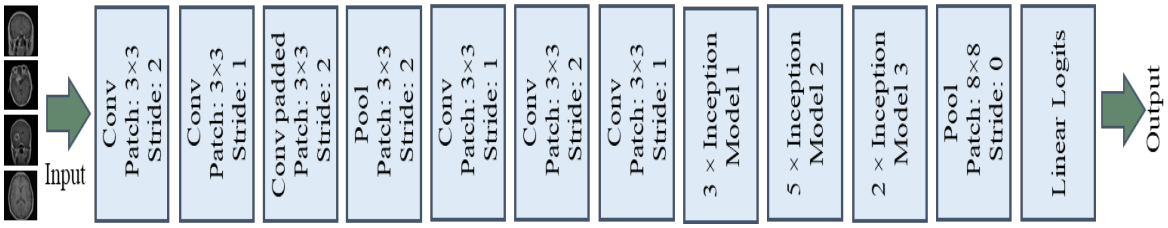

Fig. 7. Incpetion-V3 block/architecture diagram

2.4. Performance Calculation

After fitting/training the models, we utilized test data to estimate their performance. The metrics that were calculated for performance evaluation are listed below. We identified the model that could predict the outcome best using these parameters. Many percentage performance metrics [29] have been generated using Equations (1) to (7) based on the confusion matrix (CM) provided by the model.

$$Accuracy = \frac{True\ Positive + TrueNegative}{Total\ Number\ of\ Sentiment} \times 100\% \quad (1)$$

$$True\ Positive\ Rate\ (TPR)\ or\ Recall = \frac{True\ Positve}{True\ Positive + False\ Negative} \times 100\% \quad (2)$$

$$True\ Negative\ Rate\ (TNR) = \frac{True\ Negative}{False\ Positive + True\ Negative} \times 100\% \quad (3)$$

$$False\ Positive\ Rate\ (FPR) = \frac{False\ Positive}{False\ Positive + True\ Negative} \times 100\% \quad (4)$$

$$False\ Negative\ Rate\ (FNR) = \frac{False\ Negative}{False\ Negative + True\ Positive} \times 100\% \quad (5)$$

$$Precision = \frac{True\ Positive}{True\ Positive + False\ Positive} \times 100\% \quad (6)$$

$$F1\ Score = 2 \times \frac{Precision \times Recall}{Precision + Recall} \times 100\% \quad (7)$$

3. Results and Discussion

We used a deep learning-based five transfer learning classifiers (TLCs) model to predict and classify the tumor from MRI images. A split of 80:20 was used to divide the 5712 tumor training photos and 1404 validation images. The test platform is run on an Intel Core i5 computer with 16 GB of RAM. The resolutions of each input image were scaled to 220×220, 220×220, 220×220, and 220×220 for the VGG-16, VGG-19, ResNet-50, Xception, and Inception-V3 models, accordingly. These models were employed in our study to upscale images to 220×220-pixel resolution. Pre-trained VGG-16, VGG-19, ResNet-50, Xception, and Inception-V3 model weights were used. For each model that is provided, Table 1 displays the four-class resulting confusion matrix from [30], [31] (TP, FN, FP, TN). According to the classification, the procedure can unquestionably offer precise and accurate outcomes.

We set up train, testing, and cross-validation for the transfer learning algorithm to acquire correct results on our dataset. We used Adam optimizer [32], [33] to calculate each parameter's learning ratio. After using the classification method, we constructed the confusion matrix for each machine learning

(ML) and deep learning (DL) model. The assessment for ML and a confusion matrix represents deep learning classification. It places great emphasis on metering accuracy, precision, and F1-Score. Each of the following rates is accurately calculated.

Table 1. Confusion matrices for applied five transfer learning algorithms

Model	Disease	TP	FN	FP	TN
VGG-16	Pituitary	818	48	23	515
	Meningioma	774	43	18	569
	Glioma	722	32	23	627
	No Tumor	671	53	8	672
VGG-19	Pituitary	840	55	14	495
	Meningioma	773	65	13	553
	Glioma	669	51	11	673
	No Tumor	868	22	10	504
Resnet-50	Pituitary	798	25	15	566
	Meningioma	760	12	19	613
	Glioma	744	36	26	598
	No Tumor	723	34	22	627
Xception	Pituitary	831	40	49	483
	Meningioma	854	104	24	422
	Glioma	715	127	89	474
	No Tumor	718	16	46	624
InceptionV3	Pituitary	751	22	11	620
	Meningioma	758	106	15	525
	Glioma	654	90	4	657
	No Tumor	794	44	6	560

We used 40 epochs with a batch size of 32 for VGG-16. We construct the confusion matrix and assess performance for each class when VGG-16 is completed. Table 2 shows the computed performance, while Fig. 8 shows the accuracy graph and loss.

Table 2. Performance appraisal tables by class for VGG-16

Model	Disease	Accuracy (%)	TPR (%)	FNR (%)	FPR (%)	TNR (%)	Precision (%)	F1 Score (%)
Vgg16	Pituitary	94.94	94.46	5.54	4.28	95.72	97.27	95.84
	Meningioma	95.66	94.74	5.26	3.07	96.93	97.73	96.21
	Glioma	96.08	95.76	4.24	3.54	96.46	96.91	96.33
	No Tumor	95.66	92.68	7.32	1.18	98.82	98.82	95.65

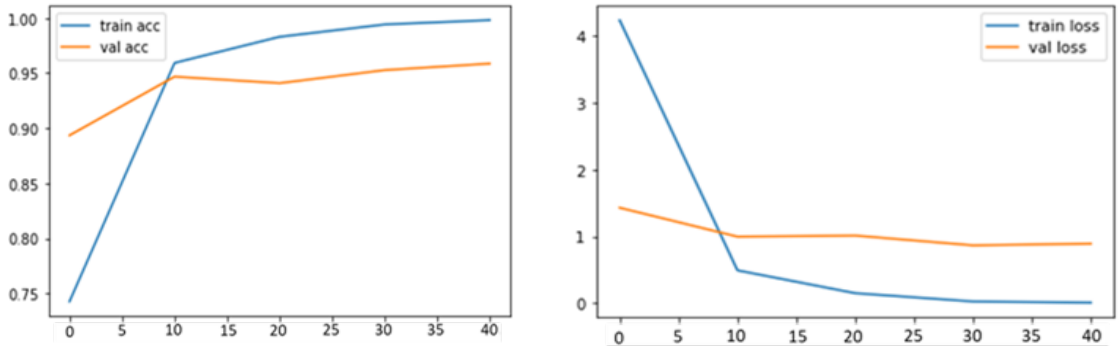

(a) (b)

Fig. 8. Diagram for (a) VGG-16 accuracy and (b) VGG-16 loss on 40 epochs

We used 40 epochs and a 32-batch size for VGG-19. We build the confusion matrix from the model after VGG-19 is finished and assess the performance of each class. The computed performance is displayed in Table 3, while the accuracy graph and loss are displayed in Fig. 9.

Table 3. Performance appraisal tables by class for VGG-19

Model	Disease	Accuracy (%)	TPR (%)	FNR (%)	FPR (%)	TNR (%)	Precision (%)	F1 Score (%)
Vgg19	Pituitary	95.09	93.85	6.15	2.75	97.25	98.36	96.05
	Meningioma	94.44	92.24	7.76	2.30	97.70	98.35	95.20
	Glioma	95.58	92.92	7.08	1.61	98.39	98.38	95.57
	No Tumor	97.72	97.53	2.47	1.95	98.05	98.86	98.19

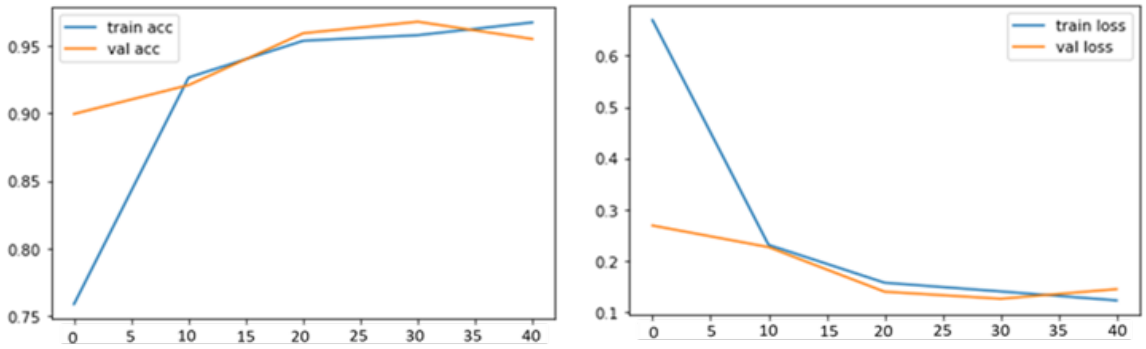

(a) (b)

Fig. 9. Diagram for (a) VGG-19 accuracy and (b) VGG-19 loss on 40 epochs

Forty epochs and a batch size of 32 were used for ResNet-50. We build the confusion matrix from the model and assess the performance of each class after ResNet-50 is finished. Fig. 10 depicts the accuracy graph and loss, while Table 4 displays the computed performance.

Table 4. Performance appraisal tables by class for ResNet-50

Model	Disease	Accuracy (%)	TPR (%)	FNR (%)	FPR (%)	TNR (%)	Precision (%)	F1 Score (%)
ResNet-50	Pituitary	97.15	96.96	3.04	2.58	97.42	98.15	97.56
	Meningioma	97.79	98.45	1.55	3.01	96.99	97.56	98.00
	Glioma	95.58	95.38	4.62	4.17	95.83	96.62	96.00
	No Tumor	96.15	95.51	4.49	3.39	96.61	97.05	96.27

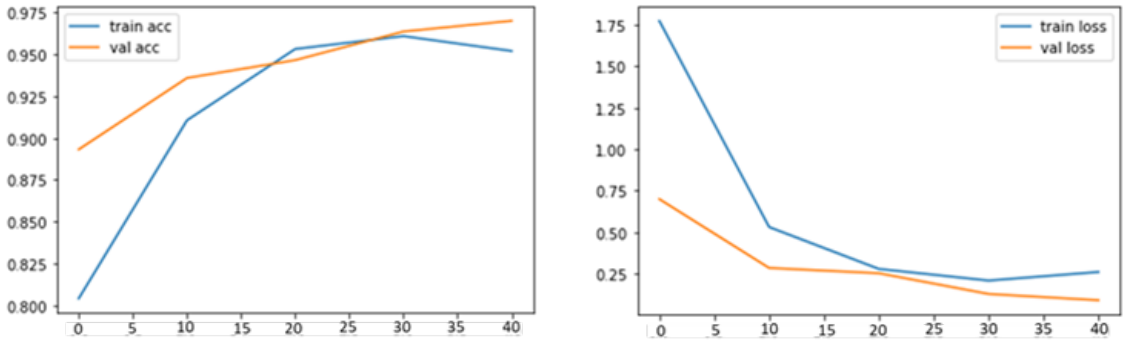

(a) (b)

Fig. 10. Diagram for (a) ResNet-50 accuracy and (b) ResNet-50 loss on 40 epochs

For Xception, we utilized 40 epochs and a batch size of 32. When Xception is completed, we create the confusion matrix from the model and evaluate each class's performance. Table 5 shows the computed performance, while Fig. 11 shows the accuracy graph and loss.

Table 5. Performance appraisal tables by class for Xception

Model	Disease	Accuracy (%)	TPR (%)	FNR (%)	FPR (%)	TNR (%)	Precision (%)	F1 Score (%)
Xception	Pituitary	93.62	95.37	4.63	9.24	90.76	94.41	94.88
	Meningioma	90.88	89.11	10.89	5.30	94.70	97.31	93.03
	Glioma	84.64	84.91	15.09	15.76	84.24	88.97	86.89
	No Tumor	95.58	97.85	2.15	6.90	93.10	93.94	95.86

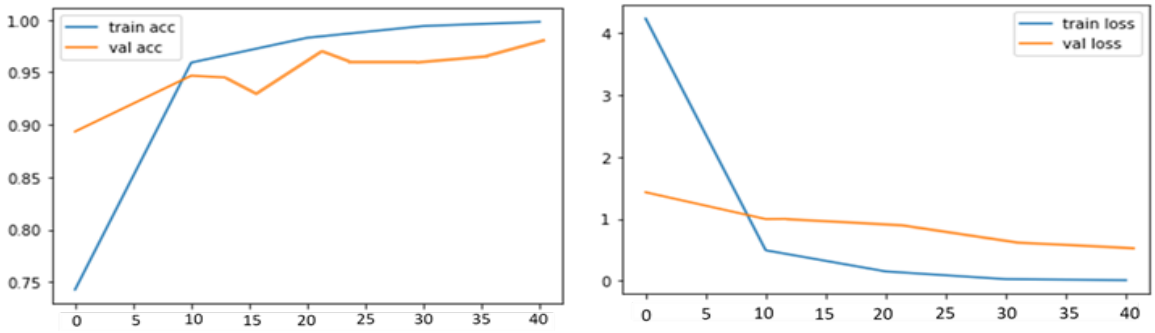

(a) (b)

Fig. 11. Diagram for (a) Xception accuracy and (b) Xception loss on 40 epochs

For Inception-V3, we utilized 40 epochs and a batch size of 32. When Inception-V3 is completed, we create the confusion matrix from the model and evaluate each class's performance. Table 6 shows the computed performance, while Fig. 12 shows the accuracy graph and loss.

Table 6. Performance appraisal tables by class for Inception-V3

Model	Disease	Accuracy (%)	TPR (%)	FNR (%)	FPR (%)	TNR (%)	Precision (%)	F1 Score (%)
Inception-V3	Pituitary	97.69	97.20	2.80	1.72	98.28	98.58	97.88
	Meningioma	91.37	87.70	12.30	2.74	97.26	98.09	92.60
	Glioma	93.34	87.95	12.05	0.60	99.40	99.40	93.32
	No Tumor	96.42	94.71	5.29	1.04	98.96	99.26	96.93

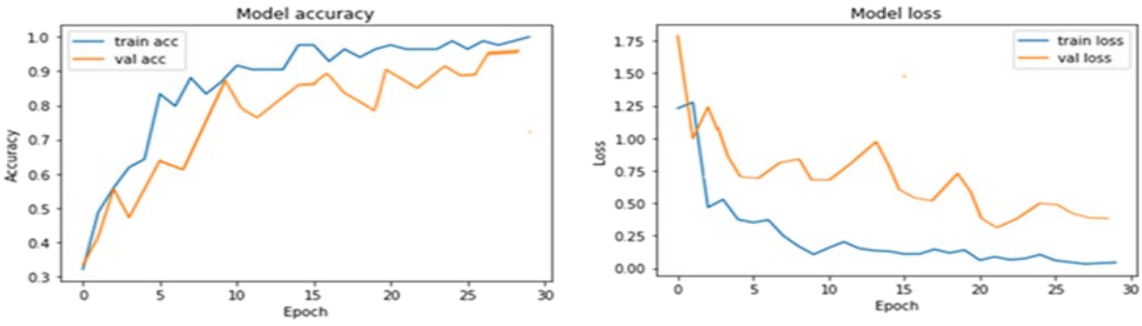

(a) (b)

Fig. 12. Diagram for (a) Inception-V3 accuracy and (b) Inception-V3 loss on 40 epochs

In this study, the performance of the trained model was evaluated using a separate test dataset. The dataset used for training the model contained both real and augmented images. The VGG-16, VGG-19,

ResNet-50, Xception, and Inception-V3 architectures were employed to train the model. After training, the model's accuracy was assessed using the test images. The weights of the pre-trained VGG-16, VGG-19, ResNet-50, Xception, and Inception-V3 models were experimented with to compare the model's performance with the other established transfer learning networks. The choice of the pre-trained network that best suited the dataset was evaluated. Table 7 lists the five unique models used in this study, and the comparison diagram for each section of the models is shown separately in Fig. 13.

Table 7. Performance appraisal tables by class for all models

Model	Accuracy	TPR	FNR	FPR	TNR	Precision	F1 Score
VGG-16	95.58	94.41	5.59	3.01	96.99	97.68	96.01
VGG-19	95.71	94.14	5.86	2.15	97.85	98.49	96.25
ResNet-50	96.67	96.58	3.42	3.29	96.71	97.35	96.96
Xception	91.18	91.81	8.19	9.30	90.70	93.66	92.67
Inception-V3	94.71	91.89	8.11	1.52	98.48	98.83	95.19

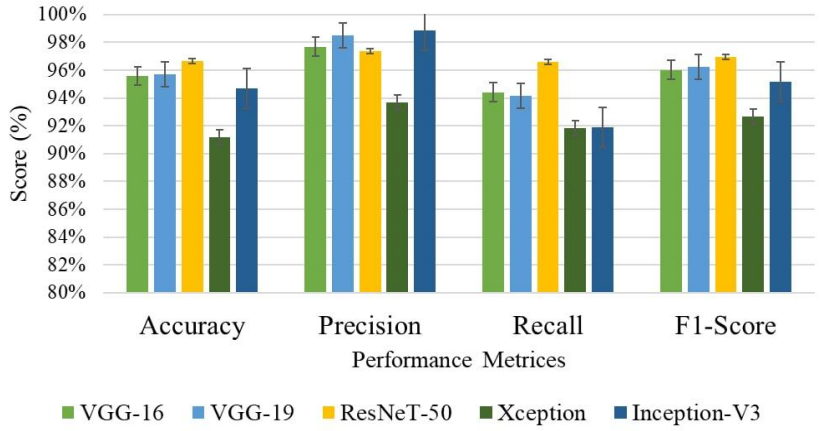

Fig. 13. Overall performance metrics for all applied TLCs

Table 8 compares our observations about detecting brain tumors with those of other writers. Previous studies have shown that raw CNN models and hybrid models can accurately detect particular types of brain tumors from MRI images with a detection rate of 84 to 92%. Comparing our results to those of other authors, we beat the previous study in identifying brain tumors with a 96.67% accuracy using 7138 Images with four groups using ResNet-50.

Table 8. Comparative analysis with previous studies

Research Work	Context	Best Method	Accuracy
Jun Cheng [34]	Brain tumor prediction via tumor region augmentation	BoW-SVM	91.28%
Ismael [35]	Brain tumor classification via statistical features	DWT-Gabor-NN	91.90%
Pashaei [36]	Brain tumor classification	CNN-ELM	93.68%
Abiwinanda [37]	Brain tumor classification	CNN	84.19%
Afshar [38]	Brain tumor classification via coarse tumor boundaries	CapsNet	90.89%
This work	**Brain tumor classification via MRI images**	**ResNet-50**	**96.67%**

4. Conclusion

The brain is one of the body's most intricate systems, with trillions of neurons interacting. The pressure inside the brain increases as a tumor develops in the head, harming the brain. A disease in which abnormal cells proliferate in the human brain is known as an intracranial neoplasm, also called a brain tumor. This work outlines CNN's classification attempts and deep feature extraction on brain tumor MRI recognition using data from Figshare and Kaggle. Here, five well-known deep CNN architectures—the VGG-16, VGG-19, ResNet-50, Xception, and Inception-V3—are used for deep feature extraction and transfer learning. The acquired dataset is precise in experimental work because

many sample photos are available. With a 96.76 percent identification rate for brain tumor MRI, ResNet50 has all models' highest accuracy. We want to increase detection accuracy in the future by utilizing a number of CNN architectural such as pertained model AlexNet, ZfNet model, and a hybrid model with adding a layer or dropping the layers. The limitation of this study recommends that inaccurate brain tumor detection from the MRI picture, which is significant scope, may be corrected in the following stages of this study by studying the non-detection image.

Declarations

Author contribution. All authors contributed equally to the main contributor to this paper. All authors read and approved the final paper.
Funding statement. None of the authors have received any funding or grants from any institution or funding body for the research.
Conflict of interest. The authors declare no conflict of interest.
Additional information. No additional information is available for this paper.

References

[1] A. M. Rauschecker *et al.*, "Artificial Intelligence System Approaching Neuroradiologist-level Differential Diagnosis Accuracy at Brain MRI," *Radiology*, vol. 295, no. 3, pp. 626–637, Jun. 2020, doi: 10.1148/radiol.2020190283.

[2] S. Pereira, A. Pinto, V. Alves, and C. A. Silva, "Brain Tumor Segmentation Using Convolutional Neural Networks in MRI Images," *IEEE Trans. Med. Imaging*, vol. 35, no. 5, pp. 1240–1251, May 2016, doi: 10.1109/TMI.2016.2538465.

[3] R. R. Laddha and S. A. Ladhake, "A Review on Brain Tumor Detection Using Segmentation And Threshold Operations," *Int. J. Comput. Sci. Inf. Technol.*, vol. 5, no. 1, pp. 607–611, 2014. [Online]. Available at : https://citeseerx.ist.psu.edu/

[4] "Brain Tumors - Classifications, Symptoms, Diagnosis and Treatments," *American Association of Neorological Surgeons*. Accessed Apr. 05, 2022. [Online]. Available at: https://www.aans.org/en/Patients/Neurosurgical-Conditions-and-Treatments/Brain-Tumors.

[5] R. Krishna and T. Menzies, "Bellwethers: A Baseline Method for Transfer Learning," *IEEE Trans. Softw. Eng.*, vol. 45, no. 11, pp. 1081–1105, Nov. 2019, doi: 10.1109/TSE.2018.2821670.

[6] D. Theckedath and R. R. Sedamkar, "Detecting Affect States Using VGG16, ResNet50 and SE-ResNet50 Networks," *SN Comput. Sci.*, vol. 1, no. 2, p. 79, Mar. 2020, doi: 10.1007/s42979-020-0114-9.

[7] F. Chollet, "Xception: Deep Learning with Depthwise Separable Convolutions," in *2017 IEEE Conference on Computer Vision and Pattern Recognition (CVPR)*, Jul. 2017, vol. 2017-Janua, pp. 1800–1807, doi: 10.1109/CVPR.2017.195.

[8] A. Y. Saleh, C. K. Chin, V. Penshie, and H. R. H. Al-Absi, "Lung cancer medical images classification using hybrid CNN-SVM," *Int. J. Adv. Intell. Informatics*, vol. 7, no. 2, p. 151, Jul. 2021, doi: 10.26555/ijain.v7i2.317.

[9] M. Shatara *et al.*, "EPCT-07. Updated report on the pilot study of using MRI-guided laser heat ablation to induce disruption of the peritumoral blood brain barrier to enhance deliver and efficacy of treatment of pediatric brain tumors," *Neuro. Oncol.*, vol. 24, no. Supplement_1, pp. i37–i37, Jun. 2022, doi: 10.1093/neuonc/noac079.135.

[10] S. Deepak and P. M. Ameer, "Brain tumor classification using deep CNN features via transfer learning," in *Computers in Biology and Medicine*, Aug. 2019, vol. 111, p. 103345, doi: 10.1016/j.compbiomed.2019.103345.

[11] M. Talo, U. B. Baloglu, Ö. Yıldırım, and U. Rajendra Acharya, "Application of deep transfer learning for automated brain abnormality classification using MR images," in *Cognitive Systems Research*, May 2019, vol. 54, pp. 176–188, doi: 10.1016/j.cogsys.2018.12.007.

[12] S. Ahuja, B. K. Panigrahi, and T. Gandhi, "Transfer Learning Based Brain Tumor Detection and Segmentation using Superpixel Technique," in *2020 International Conference on Contemporary Computing and Applications (IC3A)*, Feb. 2020, pp. 244–249, doi: 10.1109/IC3A48958.2020.233306.

[13] M. A. Khan *et al.*, "Multimodal Brain Tumor Classification Using Deep Learning and Robust Feature Selection: A Machine Learning Application for Radiologists," *Diagnostics*, vol. 10, no. 8, p. 565, Aug. 2020, doi: 10.3390/diagnostics10080565.

[14] T. Kaur and T. K. Gandhi, "Deep convolutional neural networks with transfer learning for automated brain image classification," *Mach. Vis. Appl.*, vol. 31, no. 3, p. 20, Mar. 2020, doi: 10.1007/s00138-020-01069-2.

[15] C. Srinivas *et al.*, "Deep Transfer Learning Approaches in Performance Analysis of Brain Tumor Classification Using MRI Images," in *Journal of Healthcare Engineering*, Mar. 2022, vol. 2022, pp. 1–17, doi: 10.1155/2022/3264367.

[16] Xiaoling Xia, Cui Xu, and Bing Nan, "Inception-v3 for flower classification," in *2017 2nd International Conference on Image, Vision and Computing (ICIVC)*, Jun. 2017, pp. 783–787, doi: 10.1109/ICIVC.2017.7984661.

[17] A. K. Bitto and I. Mahmud, "Multi categorical of common eye disease detect using convolutional neural network: a transfer learning approach," *Bull. Electr. Eng. Informatics*, vol. 11, no. 4, pp. 2378–2387, Aug. 2022, doi: 10.11591/eei.v11i4.3834.

[18] A. Wadhwa, A. Bhardwaj, and V. Singh Verma, "A review on brain tumor segmentation of MRI images," in *Magnetic Resonance Imaging*, Sep. 2019, vol. 61, pp. 247–259, doi: 10.1016/j.mri.2019.05.043.

[19] "Brain Tumor MRI Dataset," *Kaggle*. Accessed Apr. 24, 2022. [Online]. Available at: https://www.kaggle.com/datasets/masoudnickparvar/brain-tumor-mri-dataset .

[20] J. Mia, H. I. Bijoy, S. Uddin, and D. M. Raza, "Real-Time Herb Leaves Localization and Classification Using YOLO," in *2021 12th International Conference on Computing Communication and Networking Technologies (ICCCNT)*, Jul. 2021, pp. 1–7, doi: 10.1109/ICCCNT51525.2021.9579718.

[21] A. W. Reza, J. F. Sorna, M. M. U. Rashel, and M. M. A. Shibly, "ModCOVNN: a convolutional neural network approach in COVID-19 prognosis," *Int. J. Adv. Intell. Informatics*, vol. 7, no. 2, p. 125, Apr. 2021, doi: 10.26555/ijain.v7i2.604.

[22] H. Ali Khan, W. Jue, M. Mushtaq, and M. Umer Mushtaq, "Brain tumor classification in MRI image using convolutional neural network," *Math. Biosci. Eng.*, vol. 17, no. 5, pp. 6203–6216, 2020, doi: 10.3934/mbe.2020328.

[23] S. Hasan, G. Rabbi, R. Islam, H. Imam Bijoy, and A. Hakim, "Bangla Font Recognition using Transfer Learning Method," in *2022 International Conference on Inventive Computation Technologies (ICICT)*, Jul. 2022, pp. 57–62, doi: 10.1109/ICICT54344.2022.9850765.

[24] V. Rajinikanth, A. N. Joseph Raj, K. P. Thanaraj, and G. R. Naik, "A Customized VGG19 Network with Concatenation of Deep and Handcrafted Features for Brain Tumor Detection," *Appl. Sci.*, vol. 10, no. 10, p. 3429, May 2020, doi: 10.3390/app10103429.

[25] A. Pramanik, M. H. I. Bijoy, and M. S. Rahman, "Detection of Potholes using Convolutional Neural Network Models: A Transfer Learning Approach," in *2021 IEEE International Conference on Robotics, Automation, Artificial-Intelligence and Internet-of-Things (RAAICON)*, Dec. 2021, pp. 73–78, doi: 10.1109/RAAICON54709.2021.9929623.

[26] P. Harish and S. Baskar, "MRI based detection and classification of brain tumor using enhanced faster R-CNN and Alex Net model," *Mater. Today Proc.*, Dec. 2020, doi: 10.1016/j.matpr.2020.11.495.

[27] D. Hirahara, "Preliminary assessment for the development of CADe system for brain tumor in MRI images utilizing transfer learning in Xception model," in *2019 IEEE 8th Global Conference on Consumer Electronics (GCCE)*, Oct. 2019, pp. 922–924, doi: 10.1109/GCCE46687.2019.9015529.

[28] N. Noreen, S. Palaniappan, A. Qayyum, I. Ahmad, M. Imran, and M. Shoaib, "A Deep Learning Model Based on Concatenation Approach for the Diagnosis of Brain Tumor," in *IEEE Access*, 2020, vol. 8, pp. 55135–55144, doi: 10.1109/ACCESS.2020.2978629.

[29] M. P. Mahmud, M. A. Ali, S. Akter, and M. H. I. Bijoy, "Lychee Tree Disease Classification and Prediction using Transfer Learning," in *2022 13th International Conference on Computing Communication and Networking Technologies (ICCCNT)*, Oct. 2022, pp. 1–7, doi: 10.1109/ICCCNT54827.2022.9984286.

[30] M. J. Mia, S. K. Maria, S. S. Taki, and A. A. Biswas, "Cucumber disease recognition using machine learning and transfer learning," *Bull. Electr. Eng. Informatics*, vol. 10, no. 6, pp. 3432–3443, Dec. 2021, doi: 10.11591/eei.v10i6.3096.

[31] M. M. Fouad, E. M. Mostafa, and M. A. Elshafey, "Detection and localization enhancement for satellite images with small forgeries using modified GAN-based CNN structure," *Int. J. Adv. Intell. Informatics*, vol. 6, no. 3, p. 278, Nov. 2020, doi: 10.26555/ijain.v6i3.548.

[32] M. R. Mia, M. J. Mia, A. Majumder, S. Supriya, and M. T. Habib, "Computer Vision Based Local Fruit Recognition," *Int. J. Eng. Adv. Technol.*, vol. 9, no. 1, pp. 2810–2820, Oct. 2019, doi: 10.35940/ijeat.A9789.109119.

[33] J. S. Murugaiyan, M. Palaniappan, T. Durairaj, and V. Muthukumar, "Fish species recognition using transfer learning techniques," *Int. J. Adv. Intell. Informatics*, vol. 7, no. 2, p. 188, Jul. 2021, doi: 10.26555/ijain.v7i2.610.

[34] J. Cheng *et al.*, "Enhanced Performance of Brain Tumor Classification via Tumor Region Augmentation and Partition," *PLoS One*, vol. 10, no. 10, p. e0140381, Oct. 2015, doi: 10.1371/journal.pone.0140381.

[35] M. R. Ismael and I. Abdel-Qader, "Brain Tumor Classification via Statistical Features and Back-Propagation Neural Network," in *2018 IEEE International Conference on Electro/Information Technology (EIT)*, May 2018, vol. 2018-May, pp. 0252–0257, doi: 10.1109/EIT.2018.8500308.

[36] A. Pashaei, H. Sajedi, and N. Jazayeri, "Brain Tumor Classification via Convolutional Neural Network and Extreme Learning Machines," in *2018 8th International Conference on Computer and Knowledge Engineering (ICCKE)*, Oct. 2018, pp. 314–319, doi: 10.1109/ICCKE.2018.8566571.

[37] N. Abiwinanda, M. Hanif, S. T. Hesaputra, A. Handayani, and T. R. Mengko, "Brain Tumor Classification Using Convolutional Neural Network," in *IFMBE Proceedings*, vol. 68, no. 1, Springer Verlag, 2019, pp. 183–189, doi: 10.1007/978-981-10-9035-6_33.

[38] P. Afshar, K. N. Plataniotis, and A. Mohammadi, "Capsule Networks for Brain Tumor Classification Based on MRI Images and Coarse Tumor Boundaries," in *ICASSP 2019 - 2019 IEEE International Conference on Acoustics, Speech and Signal Processing (ICASSP)*, May 2019, vol. 2019-May, pp. 1368–1372, doi: 10.1109/ICASSP.2019.8683759.